DOI: 10.1002/cphc.200800502

Triple-Resonance Coherent Anti-Stokes Raman Scattering Microspectroscopy

Wei Min, Sijia Lu, Gary R. Holtom, and X. Sunney Xie*[a]

The wide application of fluorescence microscopy has revolutionized molecular detection and imaging with high sensitivity and specificity.[1,2] Despite these advantages, fluorescence microscopy is not applicable to non-fluorescent molecules. Thus, sensitive detection of non-fluorescent species imposes a challenge for both spectroscopy and microscopy.[3] Here we report a new nonlinear optical microspectroscopy,[4] femtosecond (fs) triple-resonance coherent anti-Stokes Raman scattering (CARS), in which the amplitude and phase of input fs laser pulses are optimally shaped to be in *triple* resonance with the molecular electronic and vibrational transitions to generate a coherent nonlinear signal beam at a new color with a highest possible efficiency. This technique combines the advantages of both coherent Raman scattering[5] and electronic resonant Raman scattering,[6] through fs pulse shaping technology.[7] The sensitivity is demonstrated to approach 10^2 non-fluorescent molecules in aqueous solution with Raman spectral identification, thus boosting the sensitivity of the reported CARS detection by 10^3 to 10^5 fold.[8]

Several fluorescence-free microscopy techniques have already been available. Spontaneous Raman microscopy probes the intrinsic molecular vibrational modes.[5] Second or third harmonic generation microscopy relies on the nonlinear optical polarizability of the bulk material induced by intense laser beams.[4] Unfortunately, these approaches are often limited by their low sensitivities due to the underlying weak optical effects. As a result, either a large number of molecules or a long acquisition time is required for a useful application. Surface enhanced Raman scattering has been demonstrated to achieve single-molecule sensitivity,[9] but it requires close contact of the sample with a metal surface and is thus not easily applied to 3D biological samples.

Coherent Raman scattering, in which molecular vibrations are driven coherently through stimulated excitation by laser beams, offers new possibilities for ultrasensitive detection due to the greatly amplified signal strength.[5] In CARS, which is the most popular technique among the coherent Raman scattering family, the beating between a pump (at ω_p) and a Stokes (at ω_s) beam actively drives the molecular oscillators at the difference frequency $\omega_p - \omega_s$. Under their joint action, a vibrational coherence, a coherent superposition between the ground state and the excited vibrational state, is created among different molecules throughout the sample. Through a further interaction with ω_p, this vibrational coherence can be converted into a coherent CARS signal at the anti-Stokes frequency $\omega_{as} = 2\omega_p - \omega_s$. Having approached a sensitivity of 10^{-3}–10^{-2} M, CARS microscopy is now recognized as a powerful tool for the investigation of fluorescence-free biological specimens.[8,10–12]

Herein we show that the sensitivity of the current CARS microscopy can be greatly improved by creating a condition of triple resonance. According to the third-order perturbation theory,[13] CARS signal I^{CARS} at ω_{as} is proportional to the following quantity [Eq. (1)] related to the molecular energy states:

$$I^{CARS} \propto \left| N \sum_{k,m,l,n} \frac{\mu_{km}\mu_{ml}\mu_{ln}\mu_{nk}}{(\omega_{mk} - \omega_p - i\gamma_{mk})(\omega_{lk} - \omega_p + \omega_s - i\gamma_{lk})(\omega_{nk} - \omega_{as} - i\gamma_{nk})} \right|^2 \quad (1)$$

where N is number of molecules, $i = \sqrt{-1}$, μ_{xy} is the transition dipole moment between states x and y, ω_{xy} is the energy difference between x and y, γ_{xy} is the homogeneous linewidth of the associated (electronic or vibrational) transition between x and y, and the permutation and summation runs over all the vibronic states of the molecule. Our triple resonance condition means that, as shown in Figure 1 a, the energy of the pump ω_p beam matches an electronic transition, ω_{mk}, from the ground state to the first electronic excited state; the anti-Stokes signal at ω_{as} also matches the electronic transition, ω_{nk}, from the first electronic excited state to the ground state; the energy difference $(\omega_p - \omega_s)$ between pump ω_p beam and Stokes ω_s beam overlaps with one or a few electronically coupled vibrational transitions, ω_{lk}, in the molecular ground state manifold. Therefore, triple resonance would minimize all three factors in the denominator of Equation (1), thus significantly enhancing the generation efficiency of the nonlinear signal. Certain aspects of the resonance effect have been utilized by several previous CARS spectroscopy studies on bulk samples but *not* with microscopy.[14–16]

We demonstrate triple-resonance CARS microspectroscopy through fs amplitude and phase shaping[7] which brings the following two significant benefits for sensitivity and specificity respectively. First, amplitude shaping assists in delivering the highest absolute triple-resonance signal from solute molecules without degrading the signal-to-background ratio. This is optimized, as predicted by Equation (1), when the bandwidths of ω_p excitation and the resulting ω_{as} signal are matching the homogeneous linewidth (on the order of 20 nm) of the molecular electronic resonance. On one hand, excitation with a too narrow band pulse (e.g. 10 ps pulse duration) sacrifices absolute resonant signal. On the other hand, an overly broad band

[a] *Dr. W. Min, S. Lu, Dr. G. R. Holtom, Prof. X. S. Xie*
Department of Chemistry and Chemical Biology
Harvard University, 12 Oxford Street, Cambridge, MA 02138 (USA)
Fax: (+1) 617 496 8709
E-mail: xie@chemistry.harvard.edu

WILEY InterScience DISCOVER SOMETHING GREAT
© 2009 Wiley-VCH Verlag GmbH & Co. KGaA, Weinheim

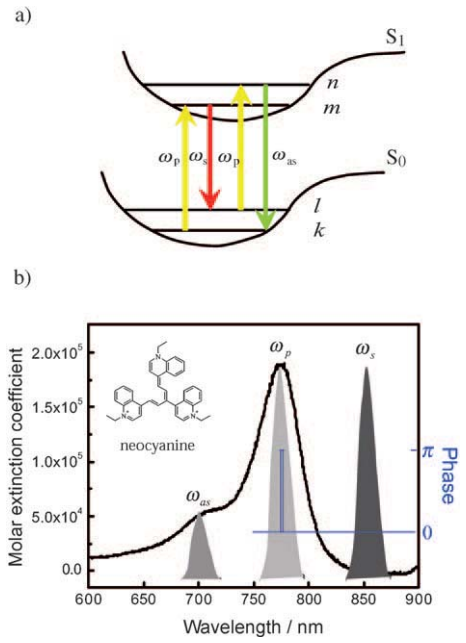

Figure 1. Triple-resonance CARS spectroscopy a) Energy diagram of the nonlinear optical process for the triple resonance CARS process. b) Amplitude- and phase-shaped excitation pulse, overlaid with the absorption spectrum of the test molecule neocyanine. The amplitude shaping involves a dual Gaussian amplitude mask creating pump ω_p and Stokes ω_s bands, while the phase shaping involves a narrow π-phase gate located at the center of pump ω_p band.

pulse (e.g. 10 fs pulse duration) excites more non-resonant background than resonant signal, as the electronic resonance is largely detuned for much of the broadband ω_p and ω_{as} components. Second, phase shaping could allow the identification of narrowband Raman spectral signature in the fingerprint region through spectral interferometry.[17–19] Without this, Raman spectral information would be masked by the broadband excitation required by the above bandwidth matching condition. Therefore, the combination of amplitude and phase shaping gives rise to both detection sensitivity and spectral specificity.

Neocyanine is selected as the test molecule because of its intense absorption ($\varepsilon \sim 180\,000\ M^{-1}cm^{-1}$) and short excited lifetime (a few ps) due to fast internal conversion rate from the electronic excited state. Its molecular structure, together with the measured absorption spectrum, is shown in Figure 1b. Like most of the cyanine chromophores, neocyanine exhibits a few electronic coupled Raman transitions in the $1100 \sim 1500\ cm^{-1}$ fingerprint region due to the favorable Frank–Condon factor. Such a vibrational coupling is then reflected in the absorption spectrum as a pronounced peak located around 700 nm.

The schematic of the optical setup, which enables fs amplitude and phase shaping, is drawn in Figure 2. A double Gaussian amplitude mask selects a pump band and a Stokes band each with about 20 nm FWHM. The resulting laser spectral amplitude is shown in Figure 1b, overlaid with the absorption spectrum. The femtosecond triple resonance condition is therefore fulfilled as follows: the excitation pump ω_p band overlaps with the electronic absorption peak around 770 nm;

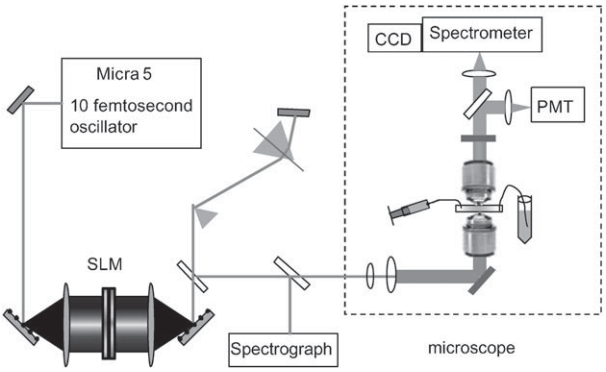

Figure 2. Experimental apparatus for triple-resonance CARS microspectroscopy. The mode-locked pulse train goes through a spatial light modulator (SLM), for both amplitude and phase shaping, before being sent into the microscope.

the signal anti-Stokes ω_{as} band overlaps with the vibronic absorption peak around 700 nm; the energy difference ($\omega_p - \omega_s$) between the broad pump ω_p and the Stokes ω_s bands spanning over the 500 cm^{-1} range center around 1300 cm^{-1}, covers one (or a few) electronic coupled vibrational transitions in the $1100 \sim 1500\ cm^{-1}$ fingerprint region.

We first record the generated CARS signal spectrum using a transform limited double-Gaussian amplitude shaped pulse. Figure 3a plots the collected forward CARS spectra for a series of neocyanine solutions. At low concentrations, the non-resonant background from ethanol solvent dominates, but at 5 μM the neocyanine signal is detectable. The fact that all the CARS spectra in Figure 3a are of broadband and carry no Raman signature, is expected for a transform limited broadband pulse excitation. This is precisely the reason why additional phase shaping is needed to restore Raman information which is spectrally much narrower than the linewidth of amplitude shaped excitation pulse.

In the phase shaping mode, we create a narrow π phase gate (2 out of 128 pixels of SLM) at the center (~770 nm) of the broad pump ω_p band (as shown in Figure 1b). We then record the CARS spectra in the presence of this narrow π phase gate. Comparable to that obtained with a transform limited pulse, the CARS spectra are dramatically different. A clear peak in the high-energy side and a dip in the low-energy side are emerging in the CARS spectrum in the vicinity of 692 nm, as shown in Figure 3b. The energy difference, between this narrow peak-dip feature at 692 nm and the shaped π phase gate at 770 nm, matches well with the 1450 cm^{-1} Raman peak of ethanol solvent. As first introduced and demonstrated by Silberberg and co-workers,[17] this peak-and-dip interference feature is due to the induced change in the relative phase between the resonant Raman signal and the non-resonant background. The applied π phase gate shifts the spectral phase of the excitation pulse by π in a narrow frequency range, inducing a $\pm\pi/2$ phase shift to the resonant signal relative to the non-resonant background with which it was initially in quadrature. These two interfere constructively at the high-energy side of the gate, generating a peak, and destructively at the low-energy side, generating a dip.

 © 2009 Wiley-VCH Verlag GmbH & Co. KGaA, Weinheim

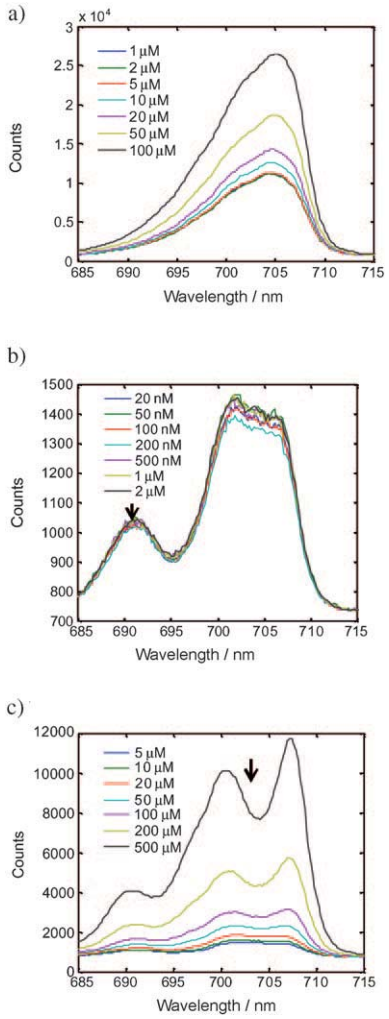

Figure 3. Triple-resonance CARS spectra. a) Excited by a transform-limited double-Gaussian-amplitude-shaped pulse but without phase shaping. The generated CARS spectra are broadband, without any narrow features, under such a transform-limited pulse excitation. b) Excited by a double-Gaussian amplitude-shaped and π-phase gate-shaped pulse: Lower concentration range, in which the resonant signal is buried in the noise of the non-resonant background from the ethanol solvent. The narrow spectral peak-dip feature around 692 nm is due to the Raman peak from ethanol. c) As in (b), excited by a double-Gaussian amplitude-shaped and π-phase gate-shaped pulse: Higher concentration range (>5 μM), in which the resonant signal goes clearly above the non-resonant background. The newly emerging peak-dip feature around 703 nm arises because of the neocyanine molecules.

What is particularly useful for this π-phase gate shaping is the new narrow spectral feature arising around 703 nm ($\sim$1250 cm^{-1} Raman peak) for neocyanine solution above 5 μM, as shown in Figure 3c. It is produced by the solute molecules rather than the plain ethanol solvent, because it becomes more and more pronounced as the concentration increases. Moreover, it is the nonlinear coherent process that gives rise to this narrow feature, as the measured spectra from either pump beam alone excitation or Stokes beam alone excitation only shows a broad featureless background from neocyanine solution. Therefore, the phase shaping allows Raman-like spectral specificity even with broadband laser excitation. Note that the narrow feature at 692 nm from ethanol solvent becomes more pronounced as the solute concentration increases (Figure 3c), because of the heterodyne amplification by the CARS signal from high concentration solute.

The recorded CARS spectra allow two different detection modes. The broadband spectra (Figure 3a) under transform limited pulse excitation provides one detection mode based on the signal intensity (Figure 4a). However, the narrow spectral feature (Figure 3c) excited under amplitude-and-phase shaped pulse provides an additional spectrum-based probe (Figure 4b). While the detection sensitivity of the intensity-based probe is limited by laser intensity fluctuations, the spectrum-based probe is shot-noise limited.

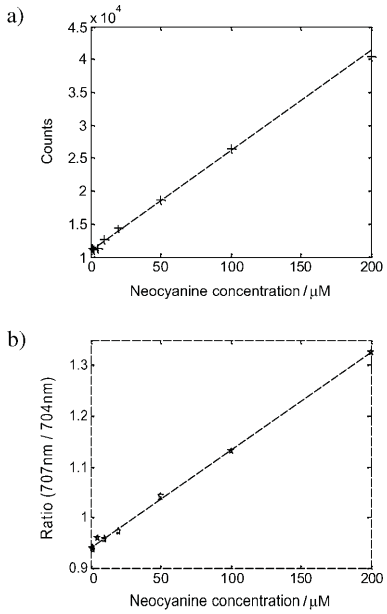

Figure 4. Concentration dependence of the triple-resonant CARS signal. a) Intensity-based probe for the spectra shown in Figure 3a. The counts are the corresponding peak values of the CARS spectra excited by the transform-limited double-Gaussian amplitude-shaped pulse. b) Spectrum-based probe for the spectra shown in Figures 3b,c. The molecular spectral feature is defined as a ratio between the spectral intensity at 707 nm and the spectral intensity at 704 nm, for the spectra excited by the double-Gaussian amplitude-shaped and π-phase gate-shaped pulse.

The concentration dependence of the signal size reveals the mechanism of the signal generation. The dependence of both intensity-based and spectrum-based probes can be roughly fitted by an empirical linear relation, shown in Figure 4, for the concentration span of 5 μM to 200 μM. When the concentration is so low that the resonant signal is smaller than the nonresonant background, one should expect the interference between the resonant and the nonresonant contribution, which results in a cross term being linear with respect to solute concentration. On the other limit where the concentration is higher than 100 μM, the self-absorption of ω_p excitation beam and ω_{as} signal by the flow cell sample itself [optical density (OD) >0.2] is significant, leading to a substantially lowered CARS signal compared to the theoretical quadratic dependence. Therefore, the combination of the above two effects

 © 2009 Wiley-VCH Verlag GmbH & Co. KGaA, Weinheim

leads to an empirical linear concentration relation over a 20-fold concentration range.

To conclude, in triple-resonance CARS microspectroscopy, the spectral amplitude and phase of fs laser pulses are shaped to optimally resonate with the molecular electronic and vibrational levels, achieving a high nonlinear signal and unique Raman spectral signature of non-fluorescent molecules. The combined advantages of coherent Raman scattering and electronic resonant Raman scattering allow a detection sensitivity of about 5 μM. This corresponds to about 300 molecules within the laser focus whose volume is estimated to be about 10^{-16} L under our high numerical aperture (N.A.) microscope objective, boosting the sensitivity of normal CARS detection by 10^3 to 10^5 fold.[8, 20] We believe that this technique has potential in studying biological chromophores with electronic transitions in the visible and UV regions,[21] such as hemoglobin, beta-carotene, cytochrome c and rhodopsin.

Experimental Section

A 15 fs pulse, centered at 810 nm with FWHM of about 100 nm, is generated from a commercial Ti:Sapphire oscillator (Micra 5, Coherent Inc.). The oscillator is optimized to have the broad bandwidth and high intensity by adjusting the prism pair inside the cavity. After being expanded by a telescope consisting of a pair of concave mirrors, the laser beam is sent into a reflective pulse shaper (Silhouette, Coherent) using a 128 pixel dual bank liquid crystal spatial light modulator SLM (CRI). SLM is configured to control both phase and amplitude of individual frequency pixels at its Fourier plane.[7] In the phase shaping mode, a narrow π-phase gate (2 out of 128 pixels) is created at the center of the broad pump ω_p band, serving as a narrow spectral probe (Figure 1 b).

A prism pair pulse compressor is installed after SLM, to pre-compensate the positive group velocity dispersion introduced by the high N.A. microscope objective. High-dispersion SF11 prisms are used whose translational and rotational adjustments are finely controlled by differential micrometers. The shaped pulse (4 mW power for pump and Stokes) is then focused with an objective (1.35 N.A. oil immersion, UPLANSAPO, Olympus) into a home-made flow cell. The liquid layer of the flow cell is about 120 μm thick, and it is continuously pumped by a syringe pump.

The triple-resonance CARS signal is generated and collected in the forward direction by another high N.A. objective (0.9 N.A., Zeiss). The collected signal is filtered by a sharp edge short pass filter (3RD710SP, Omega Optical). The filtered CARS signal is either focused onto a current-type photon multiplier tube (PMT) (Hamamatsu, R9110) with a low-noise current preamplifier (Stanford Research System, SR570) or onto the entrance slit of an imaging spectrometer (SpectroPro 150, Acton Research) equipped by a CCD camera (DV887ECS-BV, Andor). The CCD acquisition time is 3 seconds.

Acknowledgements

We are grateful to the DOE Basic Energy Sciences program (DE-FG02-07ER15875) for supporting high-sensitivity Raman detection. The instrumentation was partly supported by NSF (DBI-0649892) and the DOE Genome to Life program (DE-FG02-07ER64500).

Keywords: CARS microscopy · fluorescence-free microscopy techniques · nonlinear optics · resonance Raman scattering · vibrational coherence

[1] J. R. Lakowicz, *Principles of Fluorescence Spectroscopy, 3rd ed.*, Springer, Heidelberg, **2006**.
[2] *Handbook of Biological Confocal Microscopy* (Ed.: J. B. Pawley), Springer, New York, **2006**.
[3] W. W. Parson, *Modern Optical Spectroscopy*, Springer, New York, **2007**.
[4] *Handbook of Biomedical Nonlinear Optical Microscopy* (Eds.: B. R. Masters, P. T. C. So), Oxford University Press, Oxford, **2008**.
[5] S. Mukamel, *Principles of Nonlinear Optical Spectroscopy*, Oxford University Press, Oxford, **1999**.
[6] T. G. Spiro, *Acc. Chem. Res.* **1974**, *7*, 339.
[7] A. M. Weiner, *Rev. Sci. Instrum.* **2000**, *71*, 1929–1969.
[8] C. L. Evans, X. S. Xie, *Annu. Rev. Anal. Chem.* **2008**, *1*, 883–909.
[9] K. Kneipp, Y. Wang, H. Kneipp, L. T. Perelman, I. Itzkan, R. R. Dasari, M. S. Feld, *Phys. Rev. Lett.* **1997**, *78*, 1667–1670.
[10] A. Zumbusch, G. R. Holtom, X. S. Xie, *Phys. Rev. Lett.* **1999**, *82*, 4142.
[11] J. X. Cheng, X. S. Xie, *J. Phys. Chem. B* **2004**, *108*, 827.
[12] M. Müller, A. Zumbusch, *ChemPhysChem* **2007**, *8*, 2156–2170.
[13] Y. R. Shen, *The Principles of Nonlinear Optics*, Wiley, New York, **1984**.
[14] J. R. Nestor, T. G. Spiro, G. Klauminzer, *Proc. Natl. Acad. Sci. USA* **1976**, *73*, 3329–3332.
[15] M. D. Levenson, S. S. Kano, *Introduction to Nonlinear Laser Spectroscopy*, Academic Press, Boston, **1988**.
[16] S. F. Hanna, W. D. Kulatilaka, Z. Arp, T. Opatrny, M. O. Scully, J. P. Kuehner, R. P. Lucht, *Appl. Phys. Lett.* **2003**, *83*, 1887–1889.
[17] D. Oron, N. Dudovich, Y. Silberberg, *Phys. Rev. Lett.* **2002**, *89*, 273001.
[18] B. C. Chen, S. H. Lim, *J. Phys. Chem. B* **2008**, *112*, 3653–3661.
[19] H. Li, D. A. Harris, B. Xu, P. J. Wrzesinski, V. V. Lozovoy, M. Dantus, *Opt. Express* **2008**, *16*, 5499–5504.
[20] F. Ganikhanov, C. L. Evans, B. G. Saar, X. S. Xie, *Opt. Lett.* **2006**, *31*, 1872–1874.
[21] S. A. Asher, *Handbook of Vibrational Spectroscopy, Vol. 1*, Wiley, New York, **2001**, pp. 557–571.

Received: August 4, 2008
Revised: October 26, 2008
Published online on December 29, 2008

 © 2009 Wiley-VCH Verlag GmbH & Co. KGaA, Weinheim